

The GMRT High Resolution Southern Sky Survey for pulsars and transients -II. New discoveries, timing and polarization properties

B. Bhattacharyya¹, J. Roy¹, B. W. Stappers², T. Johnson³, C. D. Ilie², A. Lyne²,
M. Malenta², P. Weltevrede², J. Chengalur¹, S. Cooper¹, B. Kaur¹, M. Keith¹, M. Kerr⁴,
S. Kudale¹, M. A. McLaughlin^{5,6}, S. M. Ransom⁷, P. S. Ray⁴

ABSTRACT

We have been conducting the GMRT High Resolution Southern Sky (GHRSS) survey for the last four years and have discovered 18 pulsars to date. The GHRSS survey is an off-Galactic-plane survey at 322 MHz in a region of the sky (declination range -40° to -54°) complementary to other ongoing low-frequency surveys. In this paper we report the discovery of three pulsars, PSRs J1239–48, J1516–43 and J1726–52. We also present timing solutions for three pulsars previously discovered with the GHRSS survey: PSR J2144–5237, a millisecond pulsar with a period $P = 5$ ms in a 10 day orbit around a $\leq 0.18 M_\odot$ companion; PSR J1516–43, a mildly recycled $P = 36$ ms pulsar in a 228 day orbit with a companion of mass $\sim 0.4 M_\odot$; and the $P = 320$ ms PSR J0514–4408 which we show is a source of pulsed γ -ray emission. We also report radio polarimetric observations of three of the GHRSS discoveries, PSRs J0418–4154, J0514–4408 and J2144–5237.

¹National Centre for Radio Astrophysics, Tata Institute of Fundamental Research, Pune 411 007, India

²Jodrell Bank Centre for Astrophysics, School of Physics and Astronomy, The University of Manchester, Manchester M13 9PL, UK

³College of Science, George Mason University, Fairfax, VA 22030, resident at Naval Research Laboratory, Washington, DC 20375, USA

⁴Space Science Division, Naval Research Laboratory, Washington, DC 20375-5352, USA

⁵Department of Physics & Astronomy, West Virginia University, Morgantown, WV 26506, US

⁶Center for Gravitational Waves and Cosmology, West Virginia University, Chestnut Ridge Research Building, Morgantown, WV 26505

⁷National Radio Astronomy Observatory(NRAO), Charlottesville, VA 22903, USA

1. Introduction

Neutron stars are accessible to observations as pulsars and provide a valuable means for probing the behaviour of matter, energy, space and time under extraordinarily diverse conditions. Studies of normal pulsars having spin period >30 ms can reveal interesting properties like glitches, profile state changes, nulling and intermittency (e.g. Lyne et al. (1996), Kramer et al. (2006)). The extreme stability of the spin of millisecond pulsars (MSPs) makes them ideal laboratories to test the physics of gravity (Lee et al. 2012). In spite of the fact that the rates of discovery of pulsars in ongoing surveys at major telescopes over the last decade have increased dramatically, the presently known population of about 2600 pulsars is less than 5% of the predicted number of detectable radio pulsars (Faucher-Giguere et al. 2006). A large fraction of the pulsars are faint sources requiring sensitive searches and improved analysis techniques for discovery. Pulsar surveys are sensitivity limited, hence the design of more sensitive instruments promises a higher discovery rate. Large arrays of many smaller telescopes is one possible strategy for sensitivity improvement and is implemented in the Giant Metrewave Radio Telescope (GMRT⁸). It is the largest array telescope at metre wavelengths and has the potential to undertake sensitive pulsar searches, a potential which was confirmed with the discovery of 23 pulsars in targeted and blind searches (Bhattacharyya et al. (2013), Bhattacharyya et al. (2016)). We have been carrying out the GMRT High Resolution Southern Sky (GHRSS) survey using the 32 MHz bandwidth GMRT Software Backend (GSB, Roy et al. (2010)) for pulsars and transients since the fall of 2013. In this paper, the 32 MHz bandwidth component of the GHRSS survey will be notated as GHRSS “phase-1”. The GHRSS phase-1 is an off-Galactic-plane ($|b| > 5^\circ$) survey at 322 MHz whose declination range of -40° to -54° complements other ongoing low-frequency surveys with the GBT⁹ and LOFAR¹⁰. The survey description and initial discovery of 10 pulsars are reported in Bhattacharyya et al. (2016, hereafter P1). Beginning in late 2017, we embarked on phase-2 of this survey with the upgraded GMRT using up to 200 MHz of bandwidth (Roy et al. 2018). The survey description and discoveries with the GHRSS phase-2 will be reported in a follow up paper.

Following the discovery of a pulsar, the next essential step is regular timing to characterize its nature, rotation properties, and companion type and orbital properties if in a binary system. Precise localisation of the newly discovered pulsars by the GMRT interferometric array reduces the discovery positional uncertainty of $\pm 40'$ to the size of the synthesized

⁸<http://gmrt.ncra.tifr.res.in>

⁹<http://arcc.phys.utb.edu/gbncc/>

¹⁰<http://www.astron.nl/lotaas>

beam of the array, $\pm 10''$ (Roy & Bhattacharyya (2013), Roy et al. (2012)). This allowed us to carry out more sensitive follow up observations with the narrower coherent array beam.

Radiation from pulsars is believed to originate from the particles streaming outward along the open field lines above the poles of an essentially dipolar magnetic field. Linear polarization at any point in the profile is related to the orientation of the magnetic field at the corresponding point of origin. In the simplest form the position angle (PA) of the linear polarization within the pulse window rotates smoothly as a function of longitude in an “S” shaped fashion described within the “rotating vector model” (Radhakrishnan & Cooke 1969). Studying the polarization of radio pulsars is important for understanding the geometry and underlying emission mechanisms. We performed polarization studies of three of the pulsars discovered with GHRSS phase-1 survey with the Parkes telescope. Section 2 of this paper details the search and timing observations with the GMRT and polarization observations with Parkes. We describe the discovery of three pulsars, PSRs J1239–48, J1516–43 and J1726–52, in Section 3.1. Section 3.2 details the timing study of PSR J0514–4408 (originally reported as J0514–4407 in P1), mildly recycled pulsar J1516–43, and MSP J2144–5237. Section 3.3 details the detection of γ -ray pulses from PSR J0514–4408 with the *Fermi* Large Area Telescope (LAT). Section 3.4 describes the polarization properties of three of the GHRSS pulsars, J0418–4154, J0514–4408 MSP J2144–5237. In Section 4 we present discussion of the results and the summary.

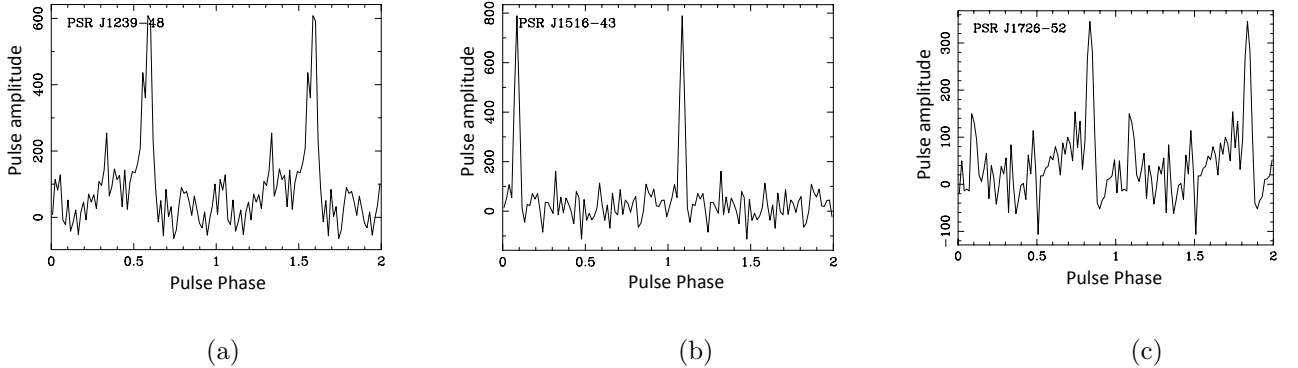


Fig. 1.— Pulse profiles (two spin periods) of three newly discovered pulsars with the GHRSS survey with 15 minutes integration at a centre frequency of 322 MHz and bandwidth of 32 MHz: (a) PSR J1239–48, (b) J1516–43, (c) J1726–52. Pulse amplitude is in arbitrary units.

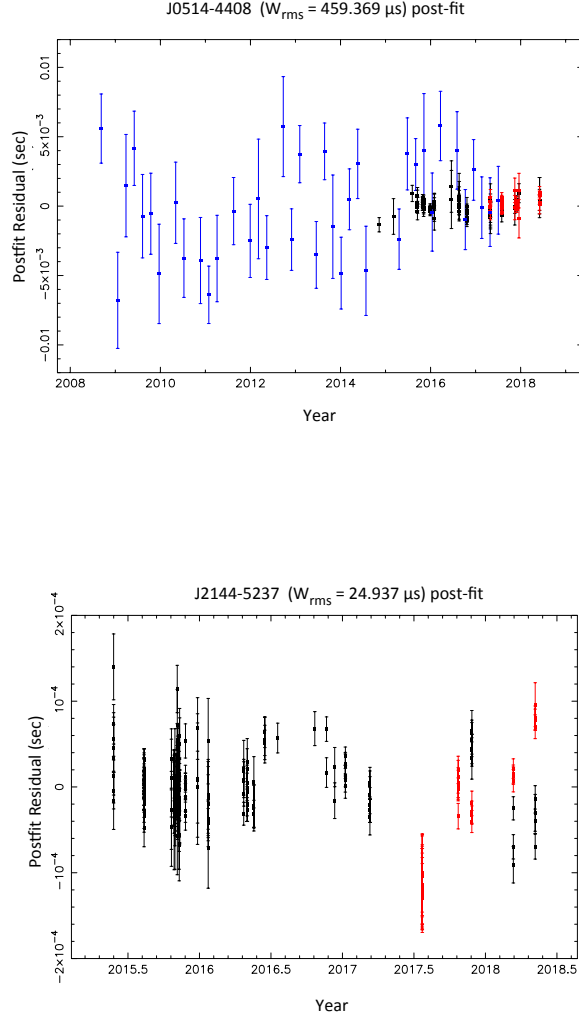


Fig. 2.— Top panel: Combined radio and γ -ray timing residuals for PSR J0514–4408. The black points represent residuals at 322 MHz with bandwidth of 32 MHz using the GMRT legacy system, the red points represent residuals at 400 MHz with a bandwidth of 200 MHz using the upgraded GMRT, the blue points represent the γ -ray timing residuals from *Fermi* LAT. Bottom panel: Radio timing residuals for PSR J2144–5237 from the GMRT observations, black and red points as in top panel.

2. Observation and analysis

The observing setup for GHRSS phase-1 is detailed in P1. The GMRT is a multi-element aperture synthesis telescope consisting of 30 antennas, each 45 m diameter, spread over a 25 km-diameter region and operating at 5 frequencies ranging from 150 MHz to 1450 MHz (Swarup et al. 1997). The observations used the GMRT Software Backend, a fully real-time backend utilizing an FX correlator¹¹ and a beamformer for an array of 32 dual polarized signals Nyquist sampled at 33 or 66 MHz (Roy et al. 2010). For the survey observations we used $\sim 61.44 \mu\text{s}$ time resolution with $\sim 16.275 \text{ kHz}$ frequency resolution over 32 MHz observing bandwidth for mid-Galactic latitudes and $\sim 30.72 \mu\text{s}$ time resolution with $\sim 32.55 \text{ kHz}$ frequency resolution over 32 MHz observing bandwidth for high-Galactic latitudes. A factor of two better frequency resolution is used at mid-Galactic latitudes to compensate for larger dispersion smearing. The calculated theoretical search sensitivity for a 15 min GHRSS pointing with incoherent array gain of 2.5 K/Jy at 322 MHz is 0.5 mJy for a 5σ detection assuming a 10% duty cycle and a total system temperature at 322 MHz of 106 K (P1; for minimum T_{sky} of GHRSS). As demonstrated in P1 (Fig. 10), the observed GHRSS survey sensitivity is within $\pm 50\%$ of the theoretical one, thus allowing us to detect faint pulsars. We recorded Stokes-I at a data rate of 32 MB/s for 8 bit samples. We used the wider incoherent beam of the GMRT (FWHM of $80'$ at 322 MHz), which is ideal for blind pulsar surveys. With 60% of the GHRSS survey ($\sim 1800 \text{ deg}^2$) we have collected about 30 TB of data. We searched for pulsations using a 512 core cluster (10 Tflops) at the National Centre for Radio Astrophysics (NCRA) and a PRESTO–based (Ransom et al. 2002) pipeline. The dedispersion range used in the search is 0 to 500 pc cm^{-3} (discussed in P1). We used an acceleration search allowing for up to 5 m s^{-2} line-of-sight acceleration for a 2 ms pulsar over 15 mins of observing duration and up to 8 harmonics were used in harmonic summing. Further details about the search analysis pipeline can be found in P1. We can localise the newly discovered pulsars and transients in the image plane with the GMRT interferometric array with an accuracy of better than $\pm 10''$ (half of the typical synthesized beam used in the image made at 322 MHz) using gated imaging of pulsars (Roy & Bhattacharyya 2013). For the pulsars which are localised in the image plane, we use the smaller field of view but more sensitive coherent array for follow up observations. Using the coherent array with the central core of the GMRT having 17 antennas (i.e. gain of $\sim 7 \text{ K/Jy}$) the timing sensitivity is 0.3 mJy for 10σ detection. After discovery we started a regular timing campaign at 322 MHz. We used the highest signal-to-noise ratio profiles as templates for extracting times-of-arrival

¹¹http://www.gmrt.ncra.tifr.res.in/gmrt_hpage/Users/doc/WEBLF/LFRA/node76.html

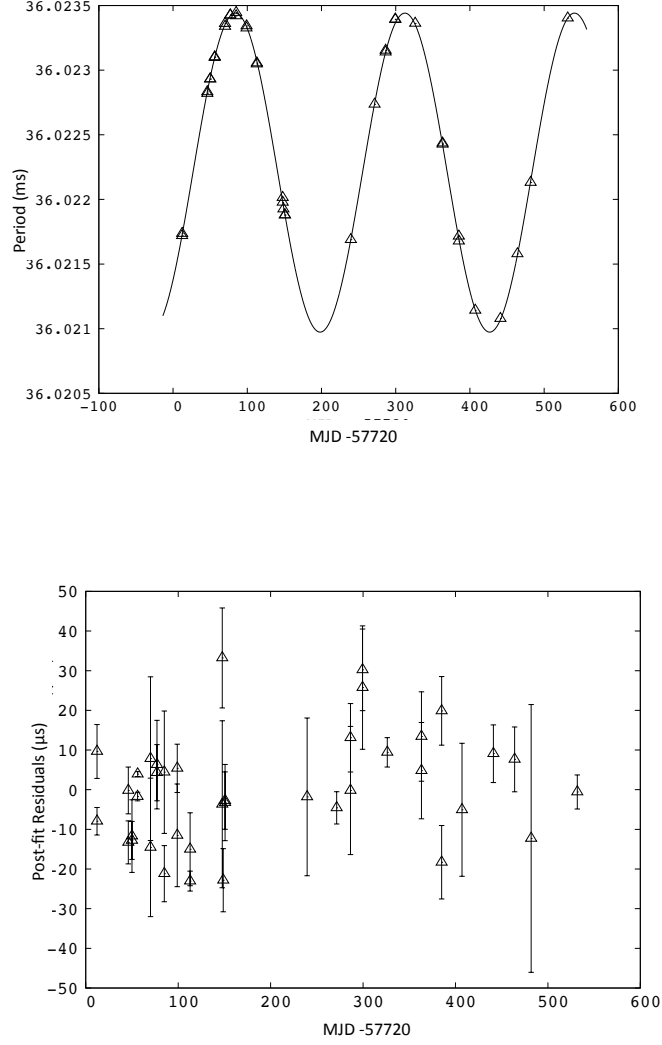


Fig. 3.— Timing studies of the mildly recycled pulsar J1516–43. Top panel: Measured pulse period variation (triangles) and fitted orbital model (solid line), Bottom panel: Post-fit residuals.

(TOAs). The TOAs are modeled using the standard pulsar timing software TEMPO2¹².

The polarimetric observations of the three GHRSS pulsars (J0418–4154, J0514–4408 and J2144–5237) were performed on the 10th of September 2017 with the Parkes radio telescope. We used the central beam of the multibeam receiver (Staveley-Smith et al. 1996) and the PDFB4 backend at a central frequency of 1369 MHz and a bandwidth of 256 MHz. More details about the receiver and the backend used in this observation can be found in Manchester et al. (2013). The receiver consists of two linear, perpendicular dipoles which receive the orthogonal components of the incoming electric field. These two fields were correlated to produce the four Stokes parameters. The first half of each observation was performed with a feed angle rotation of -45° , and the second half with a feed angle rotation of $+45^\circ$, allowing asymmetries in the performance of the two signal paths corresponding to the two polarizations to effectively cancel out. In order to calibrate for the leakage between the dipoles, a polarimetric calibration model (van Straten 2004) has been applied to the data, as derived for the Parkes Pulsar Timing Array project¹³. For some additional details about the methodology we refer to Weltevrede & Johnston (2008).

The observations were structured as follows: PSR J0418–4154 was observed for 3600 s, PSR J0514–4408 for 13500 s and PSR J2144–5237 for 12250 s (in folded mode with 30 s sub-integrations). A 120 s calibration observation with the noise diode switched on was performed before the first half and after the second half. Each half was calibrated using its corresponding polarization calibration observation. The two halves were added together to form the final integrated polarized profiles. The tools which were used to produce the plots in this section are part of the PSRSALSA¹⁴ software package (Weltevrede 2016), publicly available at the link provided.

3. Results

3.1. New discoveries

In this paper we announce the discovery of PSRs J1239–48, J1516–43 and J1726–52 in GHRSS phase-1. Fig. 1 shows the discovery profiles of these three pulsars. Table 1 presents the spin period, dispersion measure (DM) and flux density of these three pulsars marked in

¹²<http://www.atnf.csiro.au/research/pulsar/tempo2>

¹³<https://www.atnf.csiro.au/research/pulsar/ppta/>

¹⁴<https://github.com/weltevrede/psrsalsa>

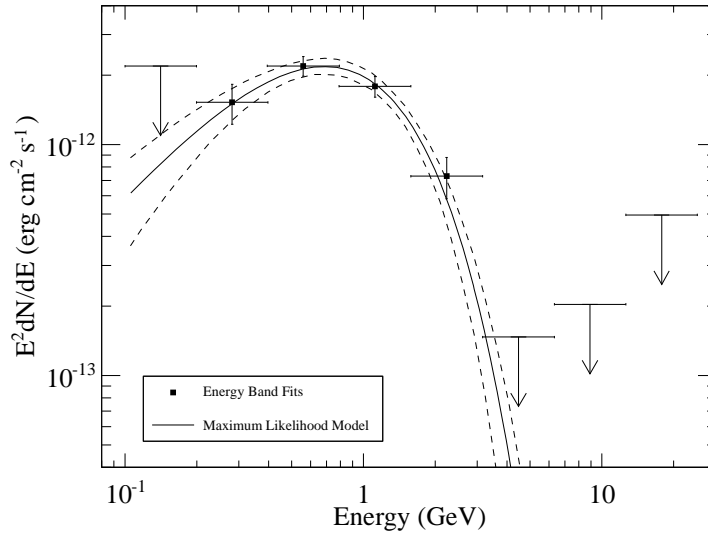


Fig. 4.— Phase-averaged γ -ray spectrum of PSR J0514–4408. The solid line is the maximum-likelihood model and the dashed lines represent the $\pm 1\sigma$ uncertainty from the fit. The points were derived from likelihood fits in the individual energy bands with the pulsar spectrum modeled as a power law with fixed photon index of 2. All uncertainties are statistical only. A 95% confidence-level upper limit is plotted for those energy bands in which the pulsar was detected with $TS < 9$ ($\sim 3\sigma$) or with < 4 predicted counts.

boldface. PSR J1239–48 is a 653.9 ms pulsar having a DM of 107.6 pc cm^{−3} and estimated discovery flux density 0.4 mJy. PSR J1516–43 has a period of 36.02 ms, a DM of 70.3 pc cm^{−3}, and a discovery flux density of 0.7 mJy. PSR J1726–52 is a 631.8 ms pulsar at a DM of 119.7 pc cm^{−3} with a flux density 0.7 mJy. Detection of such faint pulsars with the GHRSS survey indicates that we are achieving our theoretical sensitivity limit of ~ 0.5 mJy.

3.2. Timing study

We have been performing timing observations at approximately monthly cadence (with ~ 15 minutes integration) since the discovery and derived timing solutions for PSRs J0514–4408 and J2144–5237. The timing solutions for these two pulsars are presented in Table 2. We note that the timing position is off from the position derived from gated imaging. This could be due to the fact that these pulsars were observed at very low elevation angles (as the pulsars are very southern), so refractive effects can cause a significant shift between the measured position and the true position of the sources. Similar effects were also observed for other GHRSS discoveries reported in P1. The detection significance increase while pointing centre is at timing position. PSR J0514–4408 is a 320 ms pulsar with a *Fermi* LAT source 3FGL J0514.6–4406 $\sim 1.8'$ from the pulsar. Folding LAT photons with the radio timing model, we discovered γ –ray pulsations from this pulsar, described in Section 3.3. Fig. 2 presents the radio and γ –ray timing residuals for PSR J0514–4408. We have generated 38 TOAs from the *Fermi* LAT observations spanning 9.2 years, which are presented as blue points in Fig. 2. We checked the preliminary 8-year *Fermi* LAT catalog¹⁵ (The *Fermi*-LAT collaboration 2019) for positional associations with the other pulsars in Table 1 and found none. PSR J2144–5237 is a 5.04 ms pulsar in a binary with orbital period of 10.6 days for which the timing model is presented in Table 2 and timing residuals are plotted in Fig. 2. The calculated mass function (Lorimer et al. 2004) of PSR J2144–5237 is 0.002 M_⊙, which corresponds to a companion mass range of 0.18–0.46 M_⊙ considering 90° and 25° inclination and a median mass of 0.20 M_⊙ for 60° inclination.

Timing residuals for PSRs J0514–4408 and J2144–5237 contain measurements from simultaneous timing observations using the 32 MHz legacy system (black points) and the 200 MHz upgraded GMRT (red points), allowing us to determine the timing offset of 1.090011(1) seconds between them. This offset is also validated for two other GHRSS pulsars, PSRs J0418–4154 and J0702–4956, for which the timing solution is reported in P1. The timing offset of the legacy GMRT system is well characterized with the other telescopes like Parkes

¹⁵Available at https://fermi.gsfc.nasa.gov/ssc/data/access/lat/8yr_catalog/

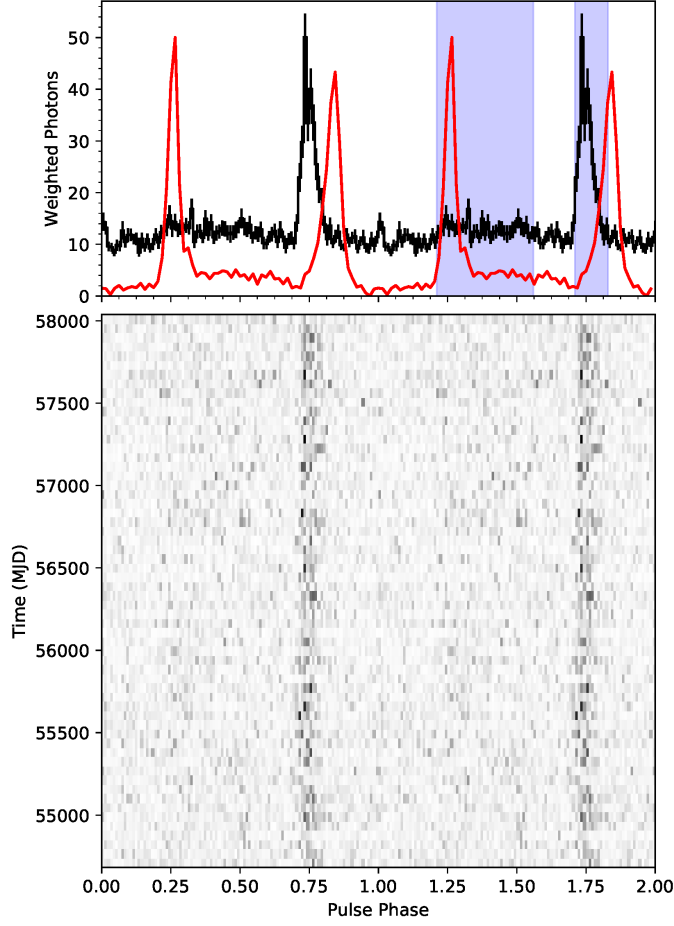


Fig. 5.— Top panel shows a 322 MHz radio profile (red) of PSR J0514–4408 plotted with the LAT γ -ray profile (using ~ 9.2 years of *Fermi* Large Area Telescope (LAT) Pass 8 data above 100 MeV). Bottom panel shows the LAT phasogram of PSR J0514–4408. The uncertainty on the DM in Table 2 is 0.006. At 322 MHz, this corresponds to an error in the DM delay to infinite frequency of $240 \mu\text{s}$ (7×10^{-4} of a pulse period)

(Roy et al. 2015), GBT, Lovell, Effelsberg (Dolch et al. 2014). Knowing the precise timing offset between 32 MHz legacy system and 200 MHz upgraded GMRT will allow combination of the upgraded GMRT data with data from other telescopes for high precision timing studies.

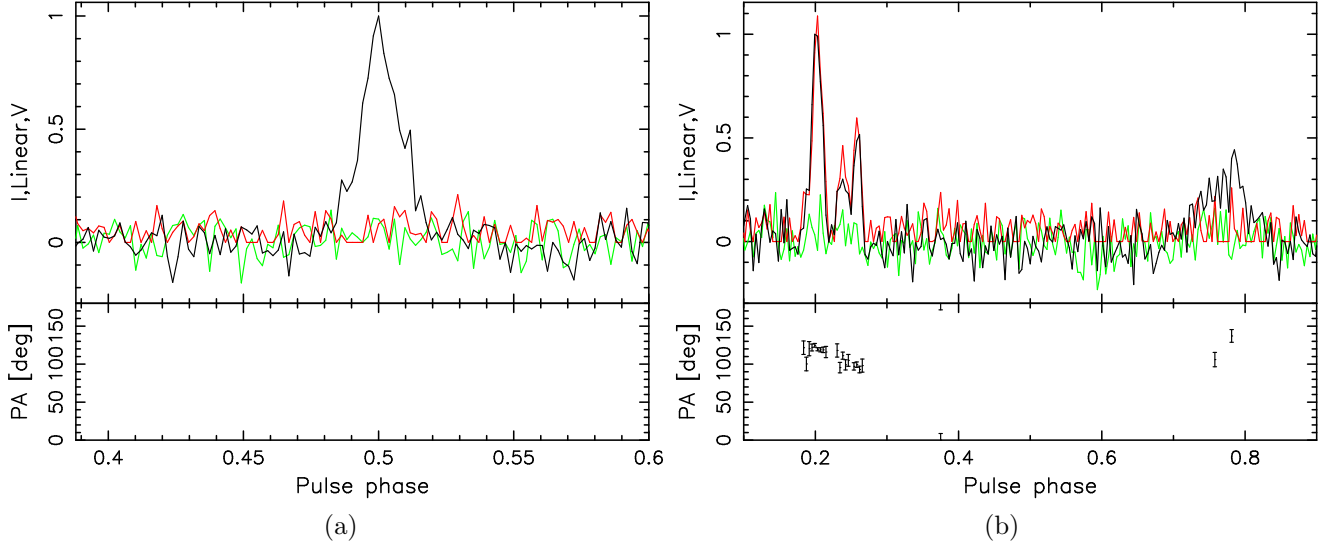


Fig. 6.— (a) Polarization pulse profile of for a 3600s Parkes telescope observation of PSR J0418–4154 at 1369 MHz center frequency with 256 MHz of bandwidth. (b) As (a) for a 13500s observation of PSR J0514–4408. In the top panel, the black solid line represents Stokes I , the red line represents the linear polarization, while the green line represents the circular polarization. The second panel shows the average position angle of the linear polarization (for all the phase bins where the linear polarization exceeds 2σ).

PSR J1516–43 is a mildly recycled pulsar in a binary orbit with an orbital period of ~ 228 days. We determined best-fit barycentric periods at various epochs using PSRTIME¹⁶. The time variations of these barycentric periods are fitted with a binary model using FITORBIT, to derive a best-fit orbital solution. The periods and model are shown in the left panel of Fig. 3. The timing model for this pulsar is presented in Table 3, but we are yet to arrive at a long-term phase-connected timing solution due to large positional uncertainty ($\pm 40'$). The mass function of $0.0225 M_{\odot}$ corresponds to a companion mass range of $0.42\text{--}1.29 M_{\odot}$ and a median mass of $0.5 M_{\odot}$ for the same inclination angle ranges as above.

¹⁶<http://www.jb.man.ac.uk/pulsar/observing/progs/psrtime.commands.html>

3.3. Discovery of γ -ray pulsations from PSR J0514–4408

3.3.1. LAT data selection and preparation

We selected Pass 8 LAT data spanning the time range from the start of science operations on 2008 August 4 up to 2017 October 12. We kept events belonging to the SOURCE class, as defined by the P8R2_SOURCE_V6 instrument response functions, with reconstructed directions within a 15° radius of the timing position of PSR J0514–4408; energies from 0.1 to 100 GeV; and zenith angles $\leq 90^\circ$ to reduce contamination of Earth limb γ rays. We filtered the events to keep only data flagged as good and recorded when the LAT was in nominal science operations mode. All analyses of *Fermi* LAT data were done using v10r00p05 of the *Fermi* ScienceTools¹⁷.

We constructed a spectral and spatial model of the region by including all sources from the third *Fermi* LAT catalog (3FGL, Acero et al. 2015) within 25° of PSR J0514–4408. For sources within 6° of PSR J0514–4408, we allowed the spectral parameters to be free only if they were found with an average significance of at least 5σ . We also allowed the spectral normalizations of sources within 8° of PSR J0514–4408 to vary if their 3FGL variability index surpassed the threshold for variability defined by Acero et al. (2015). The Galactic diffuse emission was modeled using the spectral and spatial template `gll_iem_v06.fits`, while the isotropic diffuse and misidentified cosmic-ray background emissions were modeled jointly with the spectral template¹⁸ `iso_P8R2_SOURCE_V6_v06.txt` (Acero et al. 2016). We moved the 3FGL source associated with PSR J0514–4408 to the timing position keeping all the other sources in original 3FGL positions.

The 3FGL catalog was constructed using Pass 7 reprocessed data and covers only the first four years of the mission. As such, it was necessary to check our initial fits (see Section 3.3.2) for new sources in residual counts and test-statistic (TS, Acero et al. 2015) maps, where the TS is defined as twice the difference in log-likelihood when comparing the fit without the source in the model to the fit with the source. Doing so, we found that it was necessary to free the spectral normalizations of several sources that did not meet our initial criteria (namely, 3FGL J0438.8–4519, J0515.3–4557, J0533.8–3754, J0550.3–4521, and J0428.6–3756) and that we needed to add two additional sources not in the 3FGL catalog. One of the new sources was reported already as 2FAV J0451–46.8 (Abdollahi et al. 2017).

¹⁷Available for download at
<https://fermi.gsfc.nasa.gov/ssc/data/analysis/software/>.

¹⁸Both background templates are available for download at
<https://fermi.gsfc.nasa.gov/ssc/data/access/lat/BackgroundModels.html>.

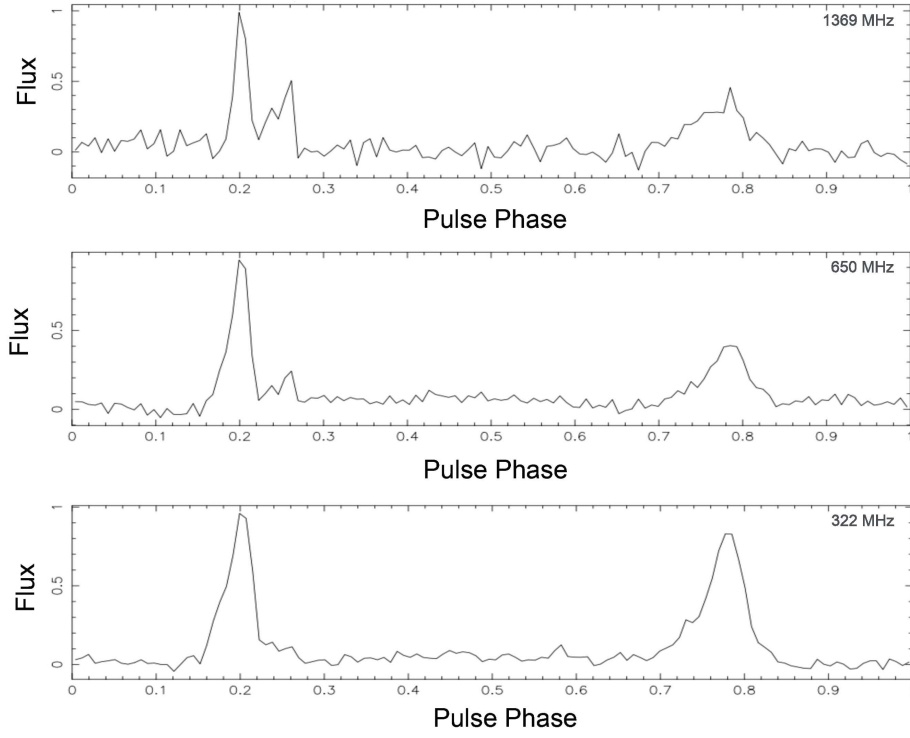


Fig. 7.— The normalized intensity profile of PSR J0514–4408 at various frequencies. The profiles at 322 and 650 MHz were observed with the GMRT, while the profile at 1369 MHz was observed with the Parkes telescope.

GeV emission from the other new source, associated with PKS 0438–43, was first reported in an Astronomer’s Telegram (Cheung 2016), with a more detailed analysis in a forthcoming paper (Cheung et al. *in preparation*).

3.3.2. LAT spectral analysis

We performed a binned maximum likelihood spectral analysis on a $20^\circ \times 20^\circ$ region, using the data and region model described in Section 3.3.1. The spectrum of PSR J0514–4408 was modeled as a power law:

$$\frac{dN}{dE} = N_0 \left(\frac{E}{E_0} \right)^{-\Gamma}, \quad (1)$$

a power law with a simple exponential cutoff:

$$\frac{dN}{dE} = N_0 \left(\frac{E}{E_0} \right)^{-\Gamma} \exp \left\{ - \frac{E}{E_C} \right\}, \quad (2)$$

and a power law with a super- or sub-exponential cutoff:

$$\frac{dN}{dE} = N_0 \left(\frac{E}{E_0} \right)^{-\Gamma} \exp \left\{ - \left(\frac{E}{E_C} \right)^b \right\}. \quad (3)$$

In Equations 1-3, N_0 is a normalization parameter with units of $\text{MeV}^{-1} \text{ cm}^{-2} \text{ s}^{-1}$; E_0 is a scale parameter, chosen to be 534 MeV, the PIVOT_ENERGY of the corresponding 3FGL source; and Γ is the photon index. In Equations 2 and 3 E_C is the cutoff energy, and the b parameter in Equation 3 is the exponential index, which controls the strength of the spectral cutoff. Note that fixing $b = 1$ returns Equation 2. The spectra of most γ -ray pulsars are well described by Equation 2, but the spectra of the brightest pulsars detected with the LAT are better fit with Equation 3 with $b < 1$, suggesting a sub-exponential cutoff (Abdo et al. 2013).

To test which model was preferred, we followed Abdo et al. (2013) and computed TS_{cut} to compare fits using Equations 1 and 2 and $\text{TS}_{b \text{ free}}$ to compare fits using Equations 2 and 3. The likelihood showed a significant preference for the simple exponential cutoff over the power law, and no strong preference for the fit with b as a free parameter. The phase-averaged best-fit spectral values, point source TS, TS_{cut} , $\text{TS}_{b \text{ free}}$, and integrated photon (F) and energy (G) fluxes are given in column 1 of Table 4. The phase-averaged γ -ray spectrum is shown in Fig. 4. The phase-averaged values of Γ and E_C reported in Table 4 are consistent with those of other γ -ray pulsars in Abdo et al. (2013) with similar characteristics. PSR J0514–4408 occupies a region of low spin-down power primarily populated by millisecond pulsars, but our best-fit Γ value is similar to those sources, further supporting that the same

emission mechanism is operating in young and recycled γ -ray pulsars. The magnetic field strength at the light cylinder of PSR J0514–4408, $B_{\text{LC}} \sim 230G$, is relatively weak compared to other known γ -ray pulsars, and our value of E_C agrees well with the trend of cutoff energy with B_{LC} noted by Abdo et al. (2013).

3.3.3. *LAT timing analysis*

We folded the γ -ray data using the radio timing solution described in Section 3.2. Then, using the best-fit model from Section 3.3.2, we computed spectral weights for each event within 3° of PSR J0514–4408, reflecting the probability that a given event should be associated with the pulsar. These spectral weights have been shown to enhance the detectability of pulsations in LAT data (Kerr 2011). Using the phase-folded and spectrally weighted events with a weighted version of the H test (de Jager et al. 1989; de Jager & Büsching 2010; Kerr 2011), we detected significant pulsations. However, analysis of the pulse phase vs. time suggested that the timing solution did not accurately describe the pulsar rotation at epochs preceding the radio discovery. Fig. 5 presents the phasogram for PSR J0514–4408. An aligned 322 MHz profile and the γ -ray LAT profile after refining the timing solution as described below, is presented in the top panel, corresponding to a detection significance of 32σ .

We fit an analytic template to the pulse profile comprising a two-sided Gaussian for the main peak and a single-sided Gaussian for the broad, second peak. We then extracted 50 TOAs by cross-correlating with the unbinned data (Ray et al. 2011), and we then produced a joint timing solution by fitting the model parameters to the radio and *Fermi* TOAs with TEMPO2. We subsequently iterated the process to produce a final analytic template and timing model¹⁹. With the final timing solution, we find that a two-peak pulse profile model is strongly preferred, with a log likelihood difference between a one- and two-peaked model of 21.39 for three extra degrees of freedom. The best-fit parameters of the γ -ray pulse profile are given in Table 5.

In order to estimate the inclination angle of its magnetic axis and that of our line of sight with respect to the spin axis of PSR J0514–4408, we used the geometric models and fitting methods of Johnson et al. (2014) and Wu et al. (2018). Our initial attempts, assuming a simulated spin period of 100 ms, period derivative of $1 \times 10^{-15} \text{ s s}^{-1}$, and radio frequency of 300 MHz; were unsuccessful at simultaneously matching the observed γ -ray and radio

¹⁹The final timing solution will be available at
<https://fermi.gsfc.nasa.gov/ssc/data/access/lat/ephems/>.

pulse profiles. However, as discussed in Section 3.4.2, there is reason to think that the radio emission originates at a relatively high altitude in the magnetosphere ($\gtrsim 1130$ km). The simulated radio pulse profiles we use follow the model of Story et al. (2007), which (using the radius to frequency mapping of Kijak & Gil 2003) place the 300 MHz emission at an altitude of 270 km (assuming a neutron star radius of 10 km). We generated new simulated radio pulse profiles, with emission at an altitude of 1130 km, and performed new fits. These new fits matched the γ -ray profiles well for moderate inclination and viewing angles, but the fits to the radio profile were still not satisfactory and suggested a higher altitude might still be needed.

In order to investigate the spectral behavior in each peak, we employed a modified Bayesian blocks (Scargle 1989; Jackson et al. 2005; Scargle et al. 2013) analysis to define the relevant phase intervals for the γ -ray pulse profile, with 100 phase bins per rotation. Our method used the weighted counts profile, similar to what was done by Caliendo et al. (2013) but using a weighted average when deciding whether or not to split a block. We reproduce the γ -ray pulse profile over the phase range -1 to 2 and use an f-test, with a χ^2 statistic, to test if the data are best described by one block or two, requiring that the probability of incorrectly splitting one block into two be ≤ 0.05 . If we split the block into two, we then test the leftmost (earlier phase) block to see if it should be split or not, stopping when the f-test suggests one block is sufficient or the block reaches the minimum size we impose of 5 phase bins. This process moves to later phases and continues until there are no more blocks to test.

Using this method, we defined three phase intervals of interest. We denoted the highest γ -ray peak as peak 1, defined to be phases $\phi \in [0.71, 0.83]$. A broader, but lower amplitude peak 2 is defined as $\phi \in [0.21, 0.58]$. These two peaks are indicated by the blue shaded region in Figure 5. The final phase interval, the off-peak, was defined as $\phi \in [0.0, 0.21) \cup (0.58, 0.71) \cup (0.83, 1.0)$. We performed binned maximum likelihood fits in each phase interval, accounting for the difference in exposure. We started with the best-fit model from the phase-averaged analysis described in Section 3.3.2, but only let the normalizations of other sources within 3° be free to vary. The normalization of the isotropic diffuse component was allowed to vary, but the spectral parameters of the Galactic diffuse component were held fixed. The results for both peak 1 and peak 2 are given in columns 3 and 4 of Table 4, with the likelihood strongly favoring the power-law with a simple exponential cutoff shape in both cases.

The best-fit photon index of peak 1 is harder than peak 2, but the difference is not significant. Aside from the flux difference, the spectra in the peaks are compatible. There was no significant detection in the off-peak phase interval, $TS = 5$ assuming a power-law shape. We calculate a 95% confidence-level upper limit on the integrated photon flux, 0.1 to

100 GeV, of $5.3 \times 10^{-9} \text{ cm}^{-2} \text{ s}^{-1}$ on any non-pulsed γ -ray emission, correcting the exposure to a phase-averaged value.

From the best-fit spectrum for the phase-averaged γ -ray data, we can derive a γ -ray luminosity of $L_\gamma = 4\pi f_\Omega G d^2 = (9.61 \pm 0.85) \times 10^{32} \text{ erg s}^{-1}$, using a beaming factor of $f_\Omega \sim 1$ (Abdo et al. 2013), the DM-derived distance (d), and the energy flux (G). Assuming a neutron star moment of inertia of $1 \times 10^{45} \text{ g cm}^2$, the timing parameters in Table 2 yield a spin-down power for PSR J0514–4408 of $\dot{E} = 2.45 \times 10^{33} \text{ erg s}^{-1}$. This implies an efficiency of converting rotational energy into γ -rays of $\eta_\gamma = L_\gamma/\dot{E} = 0.39 \pm 0.03$, which agrees well with other known γ -ray pulsars with similar \dot{E} (Abdo et al. 2013).

3.4. Polarization and multi-frequency study

3.4.1. PSR J0418–4154

The polarimetric pulse profile of PSR J0418–4154 at a center frequency of 1369 MHz and a bandwidth of 256 MHz obtained from an observation of 3600 s duration with the Parkes telescope is displayed in Fig. 6a. This pulsar appears to be unpolarized at our observing frequency. Fitting for Rotation Measure (RM) was attempted but no significant value was measured.

3.4.2. PSR J0514–4408

The polarization pulse profile of PSR J0514–4408 at 1369 MHz is displayed in Fig. 6b. The main pulse (MP), which peaks at pulse phase 0.2, appears to be completely linearly polarized, with no significant circular polarization, while the interpulse (IP) is unpolarized. The PA swing in the MP is relatively shallow and smooth, with no orthogonal polarization mode (OPM) jumps. Given the lack of detail in the shape of the PA swing and the fact that we only detect enough significant PA points for the MP, fitting the Rotating Vector Model (Radhakrishnan & Cooke 1969, RVM) to the swing was not constraining.

We can infer more about the geometry of this pulsar by looking at the frequency evolution of the total intensity profile, displayed in Fig. 7. The profiles at 322, 650 and 1369 MHz were aligned using the leftmost component of the MP, so that this feature was always at phase 0.2. The change in profile shape at phase 0.18, seen at all frequencies, indicates that we correctly identified and aligned the same components in the plots.

Although we observe a MP and IP, it does not automatically follow that the pulsar is an orthogonal rotator, and that what we observe is radiation coming from both magnetic poles. The separation between the MP and IP is more than 0.5 phase. Thus, it could be the two sides of a wide beam centered on a magnetic axis at a low inclination angle of the magnetic axis relative to the rotation axis. This could be taken as evidence in favor of a wide profile and a low magnetic inclination angle. The strong indicator of it being an orthogonal rotator, however, is that the separation between the two peaks remains constant as a function of frequency. In general the emission height is thought to be a function of frequency, which should change the separation of the components observed from the same pole (Lorimer et al. 2004). For this pulsar, we see significant profile evolution with frequency but the separation between the MP and the IP remains unaffected. Another indication of it being an orthogonal rotator is the lack of significant bridge emission in between the MP and IP at any frequency. We do not see any sign of bridge emission being present in 322, 650 and 1369 MHz, although our flux limit is not particularly constraining.

The MP of this pulsar looks like a single peaked component at 322 MHz with weak structure on the trailing edge of the pulse. From Fig. 7, we can see that with increasing frequency the structure evolves into two peaks. This indicates that the fiducial plane crossing (the plane containing both the rotation and the magnetic axis) might be at a later pulse phase than initially inferred from the 322 MHz profile. Furthermore, by looking at the IP we see that the profile is asymmetrical at all observed frequencies, as the leading edge has a slower rise compared to the trailing edge. This might indicate that the fiducial plane crossing is at an earlier pulse phase with respect to where the IP peaks. This would explain the deviation from 0.5 phase difference between the MP and IP, as should be the case if we see opposite poles of the neutron star.

That PSR J0514–4408 may be an orthogonal rotator is consistent with the classical γ -ray models (e.g. Watters 2009) predicting that a large fraction of orthogonal rotators can be detected. Nevertheless, Rookyard et al. (2015a) obtained a distribution of inclination angles for 28 γ -ray loud pulsars, and observed an unexpected skewness towards low values. Despite this skew, a number of pulsars with higher α (angle between the rotation and magnetic axis) are present in their sample. For example, PSRs J0908–4913 and J1057–5226 from their sample have interpulses and higher values of α .

Since the PA swing of the MP is relatively flat, we can measure the steepest gradient by fitting a straight line, and we obtain (-1.1 ± 0.1) . If PSR J0514–4408 is an orthogonal rotator, as discussed before, we consider the closest approach of the line-of-sight to the magnetic axis to occur somewhere within the MP, and the steepest region of the PA gradient (inflection point) to occur in this region as well, as predicted by the RVM. Our value for the

Table 1: Parameters of the pulsars discovered in the GHRSS survey and studied in this paper

Pulsar name	Period (ms)	Dispersion measure (pc cm ⁻³)	Detection significance (σ)	Flux density [†] (mJy)
PSR J0418–4154	757.11	24.325(9)	50	10.3
PSR J0514–4408	320.27 [‡]	15.122(6)	42	9.7
PSR J1239–48	653.9	107.6	21	0.4
PSR J1516–43	36.02	70.3	9	0.7
PSR J1726–52	631.8	119.7	8	0.7
PSR J2144–5237	5.04	19.5465(2)	9	1.6

We announce the discovery of the pulsars marked in bold face in this paper.

Uncertainty in dispersion measure value in the last digit are quoted in the parentheses for the pulsars for which accurate measurement is possible with long-term timing

[†] : Flux density is without primary beam correction for the three newly discovered pulsars.

[‡] : Please note that there was a typo in the period mentioned for this pulsar in P1.

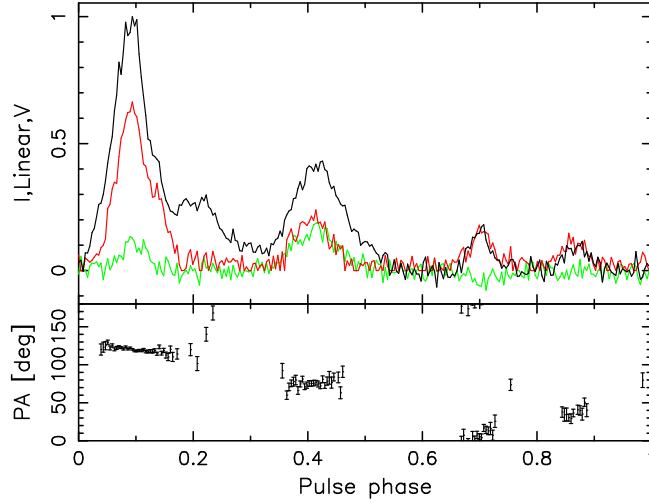


Fig. 8.— Polarization pulse profile for a 12250s observation of PSR J2144–5237, as Figure 6a.

Table 2: Timing parameters of PSR J0514–4408 and J2144–5237

Name	J0514–4408	J2144–5237
Gated imaging position*		
Right ascension (J2000)	05 ^h 14 ^m 51 ^s .84(1 ^s .04)	21 ^h 44 ^m 39 ^s .2(65 ^s .7)
Declination (J2000)	−44°07′06″.51(8″.4)	−52°37′32″.17(3″.8)
Parameters from radio and γ -ray timing*		
Right ascension (J2000)	05 ^h 14 ^m 52 ^s .190(3)	21 ^h 44 ^m 35 ^s .65(6)
Declination (J2000)	−44°08′37″.38(2)	−52°37′07″.53(2)
Pulsar frequency f (Hz)	3.122357486324(6)	198.3554831467(9)
Pulsar frequency derivative \dot{f} (Hz s ^{−1})	−1.99080(1)×10 ^{−14}	−3.50(2)×10 ^{−16}
Period epoch (MJD)	57330	57328
Dispersion measure DM [†] (pc cm ^{−3})	15.122(6)	19.5465(2)
Binary model	—	ELL1
Orbital period P_b (days)	—	10.5803185(2)
Projected semi-major axis x (lt-s)	—	6.361098(1)
Epoch of ascending node passage T_{ASC} (MJD)	—	57497.785577172346066(1)
Timing Data Span	54715.2–58271.5	57167.9–58245.1
Number of TOAs	155	217
Reduced Chi-square	1.4	2.9
Post-fit residual rms (ms)	0.459	0.024
Derived parameters		
Period (ms)	320.270822408985(6)	5.04145377851813(2)
Period Derivative (s/s)	2.04203(2)×10 ^{−15}	8.89(7)×10 ^{−21}
Total time span (yr)	9.7	2.9
Spin down energy loss rate \dot{E} (erg/s)	2.4×10 ³³	2.7×10 ³³
Characteristic age (yr)	2.5×10 ⁶	8.9×10 ⁹
Surface magnetic flux density (Gauss)	8.2×10 ¹¹	2.1×10 ⁸
Rotation measure (rad m ^{−2})	17.3	25.1
DM distance (kpc) [‡]	0.8	0.8
DM distance (kpc) ^{‡†}	0.9	1.6

* Errors correspond to 1 σ .

[†] DM values are calculated from fitting sub-band TOAs from 300–500 MHz wide observing band of uGMRT

[‡] using the Cordes & Lazio (2001) model of electron distribution

^{‡†} using the Yao et al. (2017) model of electron distribution

We note that the calculated DM distance is model dependent.

Timing uses DE421 solar system ephemeris.

Table 3: Timing parameters of PSR J1516–43

Right ascension (J2000)	15 ^h 16 ^m 32 ^s 31(1 ^s .09)
Declination (J2000)	−43°20′00″00(1″0)
Pulsar frequency f (Hz)	27.760652(2)
Period epoch (MJD)	57575.4
Dispersion measure DM (pc cm ^{−3})	70.3
Binary model [†]	BT
Orbital period P_b (days)	228.4(1)
Projected semi-major axis x (lt-s)	1.0(1)
Epoch of ascending node passage T_{ASC} (MJD)	57575.419(1)
Number of TOAs	40
Reduced Chi-square	1.04
Derived parameters	
Period (ms)	36.022209(2)
DM distance (kpc) [‡]	1.8
DM distance (kpc) ^{‡†}	3.0
Total time span (yr)	520 days

[†] used by FITORBIT software

[‡] using the Cordes & Lazio (2001) model of electron distribution

^{‡†} using the Yao et al. (2017) model of electron distribution

We note that the calculated DM distance is model dependent.

Table 4: γ –ray spectral fit results for PSR J0514–4408

Parameter	Phase-averaged	Peak 1	Peak 2
N_0 (10 ^{−11} cm ^{−2} s ^{−1} MeV ^{−1})	1.20±0.28	0.87±0.18	0.36±0.16
Γ	0.77±0.34	0.46±0.27	1.20±0.50
E_C (MeV)	560±120	500±80	590±230
F (10 ^{−9} cm ^{−2} s ^{−1})	7.3±1.2	4.1±0.4	3.1±0.9
G (10 ^{−12} erg cm ^{−2} s ^{−1})	4.8±0.4	3.0±0.2	1.6±0.3
TS	409	883	94
TS _{cut}	178	153	46
TS _{b free}	1	0	1

Note: Column 1 reports results for the phase-averaged analysis described in Section 3.3.2. Columns 2 and 3 report results for the phase-resolved analyses for each peak in the γ -ray light curve as described in Section 3.3.3. The photon and energy fluxes reported in rows 4 and 5 are integrated from 0.1 to 100 GeV. All uncertainties are statistical only.

Table 5: γ -ray pulse profile details for PSR J0514–4408

Parameter	Value
ϕ_1	0.735 ± 0.003
$w_{1,l}$	0.014 ± 0.002
$w_{1,t}$	0.034 ± 0.0030
ϕ_2	0.393 ± 0.021
w_2	0.137 ± 0.017

Note: The peak widths (w_i) are given as half-width at half max values. For the two-sided Gaussian, $w_{1,l}$ refers to the leading side of the peak, earlier phases, while $w_{1,t}$ refers to the trailing side of the peak, later phases.

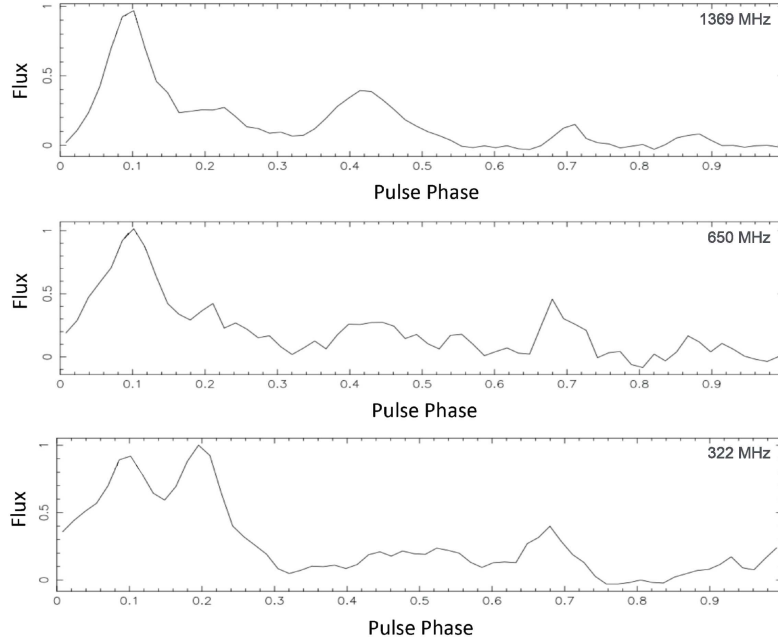


Fig. 9.— The normalized intensity profile of PSR J2144–5237 at various frequencies. The profiles at 322 and 650 MHz were observed with the GMRT, while the profile at 1369 MHz was observed with the Parkes telescope.

gradient is actually a lower limit, as the steepest gradient value could occur beyond the MP. Such a delay could arise due to relativistic effects (Blaskiewicz et al. 1991). The gradient of the steepest part of the RVM can be written in terms of the magnetic inclination angle, α , and the angle between the magnetic axis and the line-of-sight at closest approach, β , as $\sin(\alpha)/\sin(\beta)$ (Komesaroff et al. 1970). For an orthogonal rotator, $\sin(\alpha)$ is close to 1, and we can infer an upper limit on β as $\sim -65^\circ$, since β is inversely proportional to the steepest gradient.

A large value of β would imply that both emission cones are very wide ($\sim 130^\circ$). If the beams are fully illuminated, it is very hard to explain how the line-of-sight could pass the two cones of emission in such a way as to create both a narrow MP and IP. From Fig. 7, we can estimate the fractional pulse width (full width half maximum) at 1369 MHz of the leading component of MP as $W_{\text{MP}} \sim 0.07$ and of IP as $W_{\text{IP}} \sim 0.14$. Hence, as narrower beams and a lower value of β are needed to explain the observed pulse widths, the value of the steepest gradient should be higher than what we observe. As stated before, this could be the case if the steepest part of the PA swing occurs at a later pulse phase compared to the fiducial plane crossing, somewhere outside the observed MP, at least at 0.05 rotational phase delay. This delay, $\Delta\phi$, measured in radians, is predicted to be

$$\Delta\phi = \frac{8\pi h_{\text{em}}}{Pc}, \quad (4)$$

where h_{em} is the emission height measured with respect to the centre of the star, P is the period of the pulsar and c represents the speed of light (Blaskiewicz et al. 1991). Using the predicted lower limit on the rotational phase delay in Equation 4 gives a lower limit on the emission height as $h_{\text{em}} \sim 1130$ km, which is relatively high compared to other γ -loud pulsars (Rookyard et al. 2015a). From the sample of pulsars presented by Rookyard et al. (2015a), only PSR J0659+1414 had a higher emission height compared to our lower limit, indicating that the actual value of h_{em} is unlikely to be much larger than the limit.

Considering that the emission comes from a cone, which is defined by the last open magnetic field lines, one can define the angular radius of this region, θ_{em} , as

$$\theta_{\text{em}} = \arcsin \left(\sqrt{\frac{2\pi h_{\text{em}}}{Pc}} \right). \quad (5)$$

We can relate θ_{em} to the half-opening angle of the radio beam by

$$\rho = \theta_{\text{em}} + \arctan \left(\frac{\tan(\theta_{\text{em}})}{2} \right), \quad (6)$$

(e.g. Gangadhara et al. 2001). Using our predicted lower limit on h_{em} in Equation 5, and substituting the resulting value of θ_{em} in Equation 6, we infer a lower limit on the half-opening angle of the beam to be $\rho \sim 25^\circ$. This implies that the two emission beams could be at least 50° wide, which could explain the observed narrow MP and IP. Given that the two radio beams of this pulsar are still relatively wide, α does not have to be exactly 90° in order to explain the observed pulse widths. We measured a value of (17.3 ± 5.9) rad m $^{-2}$ for the RM for this pulsar using a method based on the RM synthesis technique, described in more detail by Ilie et al. (2018).

3.4.3. PSR J2144–5237

The polarization pulse profile of PSR J2144–5237 at 1369 MHz is displayed in Fig. 8. The profile appears to span the whole pulse phase consisting of five clear components. Such a wide multi-component profile is seen for some MSPs (e.g. Dai et al. 2015). The degree of linear polarization is relatively high for all components, except for the second component, at rotational phase 0.2, which appears to be unpolarized. The PA swing has a complex behaviour with different gradients and slope signs for different components, making it impossible to fit with the RVM. There are no observed OPM jumps visible in the shape of the PA curve. In general, the PA curves of MSPs do not fit the RVM model very well. However, Dai et al. (2015) managed to fit the RVM model for some pulsars in their sample using their higher frequency observations. Deviations from the model occurred when using lower frequencies, and the authors suggested that a reason for this could be that lower frequencies are generated further away from the neutron star surface. Because the magnetospheres of MSPs are so compact, these frequencies are probably generated close to the light-cylinder radius where the magnetic field deviates from a dipolar field.

The total intensity profile of PSR J2144–5237 at three different frequencies (322, 650 and 1369 MHz) is displayed in Fig. 9. The profiles were aligned based on the first (at pulse phase 0.1) and fourth (at pulse phase 0.7) components, which could be clearly identified at all frequencies and their separation did not change as a function of frequency. A slower evolution of the pulse profile with frequency, especially component separation, is observed in several MSPs (compared to normal pulsars), also likely due to their very compact magnetospheres (Kramer et al. 1999). In Fig. 9, the most striking evolution with frequency can be seen for the second component, situated at pulse phase 0.2. The RM value measured for this pulsar is (25.1 ± 1.9) rad m $^{-2}$.

4. Summary

In this paper we present the discovery of three pulsars with the GHRSS phase-1 survey, a timing study of three of the other newly discovered pulsars, the discovery of γ -ray pulsations from one of the GHRSS pulsars, and polarization results for three GHRSS pulsars.

We report the discovery of PSRs J1239–48, J1516–43 and J1726–52. Our estimates of the flux densities for the newly discovered pulsars suggests that we are achieving our theoretical sensitivity limit of ~ 0.5 mJy. The discovery of 13 pulsars in GHRSS phase-1 from 1800 square degree sky coverage indicates a discovery rate of 0.007 pulsars per square degree, which is one of the highest among the off-Galactic plane surveys (e.g. Stovall et al. (2014)).

We present timing models for PSRs J2144–5237, J0514–4408 and J1516–43 which were discovered with the GHRSS survey. PSR J2144–5237 is a millisecond pulsar with period of 5.04 ms in a 10 day orbit around a $\leq 0.18 M_{\odot}$ companion. PSR J0514–4408 discovered with the GMRT has a period of 320.27 ms and is associated with a *Fermi* LAT source emitting γ -ray pulses. The relative phase alignment between the γ -ray and radio light curve is intriguing and should provide meaningful insight into emission models for both wavelengths. A more detailed investigation is deferred to a future paper. The spin period of PSR J1516–43 is in between the bulk of the normal pulsars and millisecond pulsars and is in a wide binary (orbital period of ~ 228 days). The range of possible companion masses of $0.42\text{--}1.29 M_{\odot}$ implies that the companion could either be a white-dwarf (for low inclination angles) or a low-mass neutron star (for higher inclination angles). Considering the typical mass range of white-dwarfs and neutron stars and the most likely inclination angles, we calculate a $\sim 75\%$ probability that the companion will be a white dwarf and $\sim 25\%$ probability that the companion will be neutron star. If it were a low-mass neutron star companion with a very low orbital eccentricity then the second-born neutron star would have to have received a very small velocity kick at birth (van den Heuvel 2007). Comparing the rotational periodicities of the fully recycled MSPs and the normal pulsars, as well as the companion mass, suggests that PSR J1516–43 is a mildly recycled pulsar. It is thought that in the recycling process MSPs with massive CO/ONeMg white dwarfs are often mildly recycled with $10 < P < 100$ ms and $10^{-20} < \dot{P} < 10^{-18}$ (Tauris et al. 2012).

Folding ~ 9.2 years of *Fermi* Large Area Telescope Pass 8 data above 100 MeV using the radio timing ephemeris derived from the GMRT observations, we found a 32σ detection of γ -ray pulsations from PSR J0514–4408. Our best-fit spectral properties and derived γ -ray efficiency agree well with those of other γ -ray pulsars with similar characteristics. A phase-resolved analysis of the LAT data reveals no evidence for off-peak emission, such as what might be expected from a pulsar wind nebula.

We study the profile evolution for PSR J0514–4408 between 322, 650 and 1369 MHz. Similar MP and IP strengths are observed at 322 MHz, whereas at 650 and 1369 MHz the relative strength of the IP decreases. We report high linear polarization for the MP and unpolarised IP at 1369 MHz. We infer that PSR J0514–4408 is possibly an orthogonal rotator and discuss the consequences.

MSP J2144–5237 has a wide multi-component pulse profile. We report significant linear polarization for most of the profile components. A slower evolution of the pulse profile with frequency is observed for MSP J2144–5237 than is commonly seen in some MSPs (Kramer et al. 1999). However, one of the profile components with small linear polarization seems to exhibit significant profile evolution between 322 to 1390 MHz.

The *Fermi* LAT Collaboration acknowledges generous ongoing support from a number of agencies and institutes that have supported both the development and the operation of the LAT as well as scientific data analysis. These include the National Aeronautics and Space Administration and the Department of Energy in the United States, the Commissariat à l’Energie Atomique and the Centre National de la Recherche Scientifique / Institut National de Physique Nucléaire et de Physique des Particules in France, the Agenzia Spaziale Italiana and the Istituto Nazionale di Fisica Nucleare in Italy, the Ministry of Education, Culture, Sports, Science and Technology (MEXT), High Energy Accelerator Research Organization (KEK) and Japan Aerospace Exploration Agency (JAXA) in Japan, and the K. A. Wallenberg Foundation, the Swedish Research Council and the Swedish National Space Board in Sweden. Additional support for science analysis during the operations phase is gratefully acknowledged from the Istituto Nazionale di Astrofisica in Italy and the Centre National d’Études Spatiales in France. This work performed in part under DOE Contract DE-AC02-76SF00515.

B. Bhattacharyya acknowledges support of Marie Curie grant PIIF-GA-2013-626533 of European Union. Pulsar research at Jodrell Bank Centre for Astrophysics and Jodrell Bank Observatory is supported by a consolidated grant from the UK Science and Technology Facilities Council (STFC). B. W. Stappers and S. Cooper acknowledge funding from the European Research Council (ERC) under the European Union’s Horizon 2020 research and innovation programme (grant agreement No. 694745). M. A. McLaughlin is a member of the NANOGrav Physics Frontiers Center, supported by NSF award number 1430284. She is also supported by NSF award number 1458952. Work at NRL is supported by NASA. We thank Lucas Guillemot for reviewing our paper as LAT internal reviewer and providing very useful suggestions. We also thank Dave Thomson and Gulli Johannesson for their comments on the draft. The Parkes radio telescope is part of the Australia Telescope National Facility which is funded by the Australian Government for operation as a National Facility

managed by CSIRO. We thank VVS and S. Gole for maintaining the compute cluster at the NCRA. We thank the staff of the GMRT who have made these observations possible. We acknowledge support of GMRT operators. The GMRT is run by the National Centre for Radio Astrophysics of the Tata Institute of Fundamental Research.

REFERENCES

- Abdo, A. A., Ajello, M., Allafort, A., et al. 2013, *ApJS*, 208, 17
- Abdollahi, S., Ackermann, M., Ajello, M., et al. 2017, *ApJ*, 846, 34.
- Acero, F., Ackermann, M., Ajello, M., et al. 2016, *ApJs*, 223, 26.
- Acero, F., Ackermann, M., Ajello, M., et al. 2015, *ApJS*, 218, 23.
- Acero, F., Ackermann, M., Ajello, M., et al. 2016, *ApJs*, 223, 26.
- Bhattacharya D., van den Heuvel E. P. J., 1991, *Physics Reports*, 203, 1.
- Bhattacharyya, B.; Roy, J.; Ray, P. S., et al., 2013, *ApJ Letters*, 773, 12.
- Bhattacharyya, B.; Cooper, S.; Malenta, M., et al., 2016, *ApJ*, 817, 130
- Blaskiewicz M., Cordes J. M., Wasserman I., 1991, *ApJ*, 370, 643
- Caliandro, G. A., Hill, A. B., Torres, D. F., et al. 2013, *MNRAS*, 436, 740
- Cheung, C. C. 2016, *The Astronomer’s Telegram*, 9854, 1
- Cordes, J. M., Lazio, T. J. W., 2001 (*astro-ph/0207156*)
- Dai S., Hobbs G., Manchester R. N., et. al., 2015, *MNRAS*, 449, 3223
- de Jager, O. C. & Büsching, I. 2010, *A&A*, 517, L9
- de Jager, O. C., Raubenheimer, B. C., & Swanepoel, J. W. H. 1989, *A&A*, 221, 180
- Dolch, T., Lam, M. T., Cordes, J. et al. 2014, *ApJ*, 794, 21
- Faucher-Giguere C. A., Kaspi V. M., 2006, *ApJ*, 643, 332
- Gangadhara R. T., Gupta Y., 2001, *ApJ*, 555, 31
- Ilie C. D., Johnston S., Weltevrede P., in prep., *MNRAS*

- Jackson, B., Scargle, J. D., Barnes, D., et al. 2005, ISPL, 12, 105
- Johnson T. J., Venter C., Harding A. K., et al., 2014, ApJS, 213, 6
- Kerr, M. 2011, ApJ, 732, 38
- Kijak J. & Gil J., 2003, A&A, 397, 969
- Komesaroff M. M., 1970, Nature, 225, 612
- Kramer M., Lange C., Lorimer D. R., et al., 1999, ApJ, 526, 957
- Kramer, M., Lyne, A. G., O’Brien, J. T., et al., 2006, Science, 312, 549
- Lee, K. J., Bassa, C. G., Janssen, G. H., et al., 2012, MNRAS Letters, 423, 2642.
- Lorimer, D. R., & Kramer, M., 2004, Handbook of Pulsar Astronomy, Vol. 4. Cambridge, UK.
- Lyne, A., 1996, Astronomical Society of the Pacific Conference Series, Proceedings of the 160th colloquium of the International Astronomical Union held in Sydney; Australia; 8-12 January 1996, edited by S. Johnston, M.A. Walker, and M. Bailes, 105, 73
- Manchester, R. N., Hobbs, G., Bailes, M. et al., 2013, PASA, 30, 17
- Ransom, S. M., Eikenberry, S. S., Middleditch, J., ApJ, 124, 1788
- Ray, P. S., Kerr, M., Parent, D., et al. 2011, ApJS, 194, 17
- Radhakrishnan V., Cooke D. J., 1969, ApJL, 3, 225
- Rookyard S. C., Weltevrede P., Johnston S., 2015a, MNRAS, 446, 3367
- Rookyard S. C., Weltevrede P., Johnston S., 2015b, MNRAS, 464, 3356
- Roy J., Gupta Y., Pen Ue-Li, et al., 2010, Experimental Astronomy, 28, 55
- Roy J., Bhattacharyya B., Gupta Y., 2012, MNRASL, 427, 90
- Roy J., Ray P., Bhattacharyya, B. et al., 2015, ApJL, 800, 12
- Roy J. & Bhattacharyya B., 2013, ApJL, 765, 45
- Roy J., 2018, proceedings of IAU Symposium 337 - Pulsar Astrophysics: The Next Fifty Years

- Roy J. & Bhattacharyya B., 2013, ApJL, 765, 45
- Scargle, J. D. 1989, ApJ, 343, 874
- Scargle J. D., Norris J. P., Jackson B., et al., 2013, ApJ, 764, 167
- Stovall K., Lynch R. S., Ransom S. M. et al., 2014, ApJ, 2014, 791, 67
- Story S. A., Gonthier P. L. & Harding A. K., 2007, ApJ, 671, 713
- Staveley-Smith L., Wilson W. E., Bird T. S. et al., 1996, PASA, 13, 243
- Swarup, G., Ananthakrishnan, S., Subrahmanya, C., R., et al., 1997, in *High Sensitivity Radio Astronomy*, ed. Jackson, N., and Davis, R., J., (Cambridge: Cambridge University Press), 217
- Tauris T. M., Langer N., Kramer M., 2012, MNRAS, 425, 1601
- van Straten, 2004, ApJS, 152, 129
- van den Heuvel E. P. J., 2007, AIP Conference Proceedings, 924, 598
- Watters K. P., Romani R. W., Weltevrede P., et al., 2009, ApJ, 695, 1289
- Weltevrede P., 2016, A&A, 590, A109
- Weltevrede P. & Johnston S., 2008, MNRAS, 391, 1210
- Wu J, Clark C. J., Pletsch, H. J., et al., 2019, ApJ, 854, 99
- Yao J. M., Manchester R. N., Wang N., 2017, ApJ, 835, 1
- The *Fermi*–LAT collaboration, 2019, arXiv:1902.10045